Plasmonic Sensing of Refractive Index and Density in Methanol-Ethanol Mixtures at High Pressure

Camino Martín-Sánchez[a], Ana Sánchez-Iglesias[b], Paul Mulvaney[c], Luis M. Liz-Marzán[b,d], Fernando Rodríguez[a*]

[a] MALTA Consolider, DCITIMAC, Facultad de Ciencias, University of Cantabria, Av. Los Castros s/n, Santander, 39005, Spain
[b] CIC biomaGUNE and CIBER-BBN, Basque Research and Technology Alliance (BRTA), Paseo de Miramón 182, Donostia-San Sebastián, 20014, Spain
[c] ARC Centre of Excellence in Exciton Science, School of Chemistry, University of Melbourne, Victoria, 3010, Australia
[d] Ikerbasque, Basque Foundation for Science, Bilbao, 48013, Spain

* Corresponding author: rodriguf@unican.es

Abstract

The localized surface plasmon resonance (LSPR) of gold nanospheres dispersed in methanol-ethanol 4:1 was measured as a function of pressure up to 60 GPa. The LSPR exhibits an intense redshift with pressure in the range of 0-10 GPa, followed by a slower blueshift at higher pressures. This is because an increase in the solvent refractive index with pressure leads to a redshift of the LSPR peak wavelength while an increase in the electron density of the gold nanospheres with pressure leads to a blueshift. Solvent solidification at 10 GPa and associated non-hydrostatic effects have a negligible influence on the LSPR shifts in the case of nanospheres. Here we show that both the LSPR shifts and changes in the nanospheres absorption coefficient can be explained on the basis of Gans' model, and this enables the solvent refractive index and the density of the solvent to be determined across the hydrostatic pressure range from 0-60 GPa. Interestingly, plasmonic sensing shows no evidence of crystallization or glass phase transitions in MeOH-EtOH (4:1) solvents within the explored pressure range.

Introduction

It has been shown that application of pressure to AuNPs constitutes an efficient method to modify their physico-chemical properties through volume reduction of both the nanoparticle and surrounding medium – the pressure transmitting medium. In turn, gold nanoparticles (AuNP) can act as spectroscopic probes or sensors, to monitor changes in pressure or refractive index through changes in the localized surface plasmon resonance (LSPR) peak wavelength and the extinction coefficient.

It has been recently shown[1] that LSPR spectral shifts in gold nanorod (AuNR) solutions can be used to detect structural phase transitions in H_2O and to infer the value of the refractive index $n(P)$ of the medium in which the AuNRs are dispersed. Furthermore, the method allows phase transitions in the water to be detected as its phase

changes from: water → Ice VI → Ice VII. In this work, we analyze the suitability of the same method to obtain $n(P)$ in a methanol-ethanol (MeOH-EtOH) 4:1 mixture, as this is probably the most widely used pressure transmitting medium.[2] We explored changes in the AuNP LSPR, over a wide pressure range (0-60 GPa), far beyond the hydrostatic regime, in order to glean structural information about this archetypal pressure-transmitting medium in both the hydrostatic (0-10 GPa) and the less-explored non-hydrostatic (10-60 GPa) regimes.

This latter range is poorly understood due to the glassy state of the alcohol mixture and the difficulties to extract structural information under high pressure conditions. For this purpose, we employed spherical gold nanoparticles (AuNS) immersed in MeOH-EtOH (4:1) keeping a relatively low AuNS concentration (about 10^{13}AuNS/cm^3) to minimize aggregation effects. One important advantage of using AuNP plasmonics to study the pressure dependence of the solvent refractive index is related to this measurement method not requiring prior knowledge of the solvent mass density $\rho(P)$ or specific volume $V(P)$, or of the speed of sound $v(P)$ in the solvent. Conventional methods to obtain the pressure dependence of the refractive index of a material[3-7] based on interferometric or reflectivity measurements are more complicated and usually require knowledge of at least $V(P)$ or $v(P)$ independently, rendering the measurement of $n(P)$ difficult. Furthermore, in the case of non-crystalline solids, such as MeOH-EtOH 4:1 mixtures above 10 GPa,[2] measuring the solvent density is extremely challenging because diffraction methods become complicated, and determining the equation of state (EOS) from optical methods requires knowledge of $n(P)$.[8] Plasmonics provides a more direct measurement of $n(P)$ since the two main contributions to the LSPR shift are well known. The compression of the electron gas of the metal induces a blue shift, whereas the increase in medium refractive index induces a red shift and these effects can be readily decoupled. We used AuNS since, unlike other lower symmetry morphologies such as rods, stars, cubes, etc., spheres are less susceptible to deformation under strong non-hydrostatic conditions. Furthermore, contributions to the LSPR shifts due to stress or aggregation of the nanoparticles are minimized with AuNSs due to their lower spectral sensitivity.[9]

Hence in this study we have employed LSPR spectral shifts of AuNSs in MeOH-EtOH (4:1) to deduce the refractive index $n(P)$ of the solvent MeOH-EtOH. Measurements at high pressure allowed us to explore the existence of solid-solid structural phase transitions within the 10-60 GPa range. Furthermore, we analyzed the suitability of the Lorentz-Lorentz model to extract the pressure dependence of the MeOH-EtOH density from $n(P)$ data. Finally, we demonstrate a reversal of the initial LSPR trend, from redshift to blueshift, when the contribution from the increasing AuNS electron density becomes more important than the increase in solvent refractive index.

Experimental Section

Synthesis

Single-crystalline AuNSs with an average diameter of 19.9 nm were synthesized via a seeded growth method following the procedure established elsewhere.[10]

Chemicals: Gold (III) chloride trihydrate ($HAuCl_4$, ≥ 99%), hexadecyltrimethylammonium chloride (CTAC, 25 wt% in water), sodium borohydride ($NaBH_4$), hexadecyltrimethylammonium bromide (CTAB, ≥ 99%), L-ascorbic acid (AA, ≥ 99%), O-[2-(3-Mercaptopropionylamino)ethyl]-O′-methylpolyethylene glycol (PEG-SH, Mw: 5 kg / mol) were purchased from Sigma-Aldrich. Ethanol and methanol were purchased from Scharlab. Milli-Q water (resistivity 18.2 MΩ·cm at 25 °C) was used in all experiments.

Synthesis and ligand exchange of AuNS: Gold seeds (~ 1.5 nm) were prepared by fast reduction of $HAuCl_4$ (5 mL, 0.25mM) with freshly prepared $NaBH_4$ (0.3 mL, 10 mM) in aqueous CTAB solution (100 mM) under vigorous stirring for 2 min at room temperature, and then kept undisturbed at 27 ºC for 30 min to ensure complete decomposition of borohydride. The mixture turns from light yellow to brownish indicating the formation of gold seeds. An aliquot of seed solution (0.13 mL) was added under vigorous stirring to a growth solution containing CTAC (100 mL, 100 mM), $HAuCl_4$ (0.36 mL, 50 mM) and ascorbic acid (0.36 mL, 100 mM). The mixture was left undisturbed for 2 h at 25 °C. The solution containing 20 nm gold nanoparticles was centrifuged (8000 rpm, 2h) to remove excess of CTAC and ascorbic acid, and redispersed in CTAB 1 mM to a final gold concentration of 0.5 mM.

To replace the surfactant and transfer the gold nanoparticles into ethanol-methanol mixture, thiolated polyethylene glycol (PEG-SH, Mw: 5 kg / mol) was used. An aqueous solution of PEG-SH (19 mg dissolved in 3 mL) was added dropwise under stirring to a dispersion of gold nanoparticles (30 mL, 0.5 mM). The solution was left for 2h under stirring, and then centrifuged twice in ethanol. PEGylated gold nanoparticles were finally dispersed in ethanol.

High-Pressure measurements

High-pressure experiments were carried out in a Boëhler-Almax diamond anvil cell (DACs). The 200 μm thick Inconel gaskets were preindented to 50 μm. The 70 μm diameters holes were perforated with a BETSA motorized electrical discharge machine and used as hydrostatic chambers. The DAC was loaded with MeOH-EtOH 4:1 AuNS solutions and ruby microspheres (10-20 μm diameter) as pressure probes.[11] The solution itself acted as the pressure-transmitting medium. The pressure of the AuNPs solution was determined through the ruby R-line emission from small ruby balls inside the cavity, the spectral position of which is well calibrated with the pressure.[11,12] The hydrostaticity of the pressure-transmitting media was probed through the ruby R-line broadening (see figure S1 in the SI).

Optical absorption spectra under high-pressure conditions were collected on a home-built fiber-optic-based microscope,[13] equipped with two Cassegrain 20× reflecting objectives mounted on two independent x-y-z translational stages for the microfocus beam, the objective lens, and a third independent x-y translation stage for the DAC holder. Spectra in the ultraviolet-visible and near-infrared ranges were recorded with two spectrometers: an Ocean Optics USB 2000 and a NIRQUEST 512, employing Si- and InGaAs-CCD detectors, respectively. The I and I_0 intensities were measured in two separate experiments with the same DAC by loading it first with the nanoparticle solutions (I), and then with the corresponding solvent (I_0), covering the same pressure

range. The hydrostatic pressure range and liquid-solid pressure transition of AuNR solutions were determined from the pressure dependence of the FWHM of the ruby R-lines.

Results and discussion

Figure 1 shows representative transmission electron microscopy (TEM) images and the extinction spectrum of the AuNS colloid employed in the experiments. The AuNSs have an average diameter of (19.9 ± 0.3) nm, are coated with thiolatedpolyethylene glycol (Mw = 5 kg / mol) and present the characteristic LSPR band centered at 522 nm.

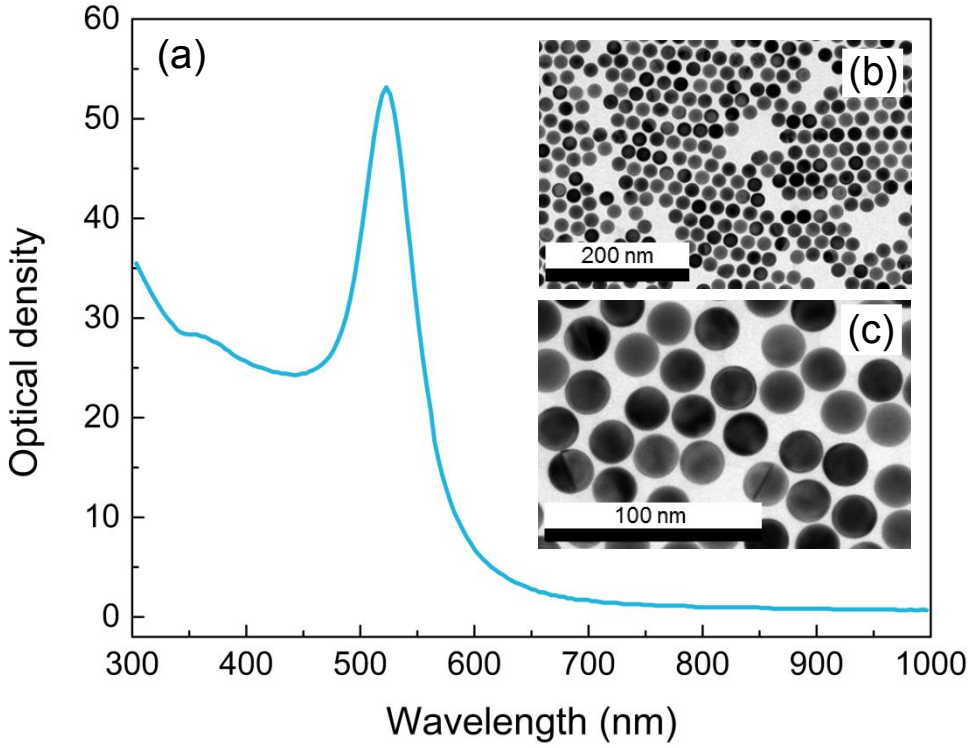

Figure 1. (a) Experimental optical extinction spectrum of the spherical nanoparticles used in the experiments (light path: 1 cm) [3.6×10^{13} NS/cm^3]. (b and c) Representative TEM images of the nanoparticles at different magnifications.

Typical variations in the extinction spectra of AuNSs in MeOH-EtOH 4:1 with pressure are shown in Figure 2. The behavior of the LSPR with pressure can be divided into two regimes: 1) an intense redshift with increasing pressure (1 nm/GPa) in the 0-10 GPa range, followed by a smoother blueshift (-0.3 nm/GPa) in the higher non-hydrostatic pressure range, 10-60 GPa. The largest LSPR shift measured at low pressure (P< 0.5 GPa) amounts to 8 nm/GPa, a smaller value compared to those previously found for AuNRs,[1,12] but more sensitive than the pressure shift of ruby (0.36 nm/GPa[11]), the most widely used high-pressure gauge.[2] Furthermore, we observe a continuous increase in the optical density at the LSPR maximum with increasing pressure, as expected from the increase in the medium refractive index and the increase in AuNS concentration due to solvent compression. Interestingly, neither the LSPR position nor the optical density at the

maximum undergo any significant change when the hydrostaticity of the solution is lost upon solvent solidification at $P = 10$ GPa (see Fig. S1 of the Supporting Information (SI)). This result is in contrast to those found in previous studies,[12] where the optical density of AuNRs showed an abrupt decrease above the solution solidification pressure, or how the LSPR of AuNRs in water undergoes abrupt variations associated with structural changes along water → Ice VI → Ice VII phase transitions, making plasmonics a suitable tool to detect structural changes of the surrounding media.[1,14]

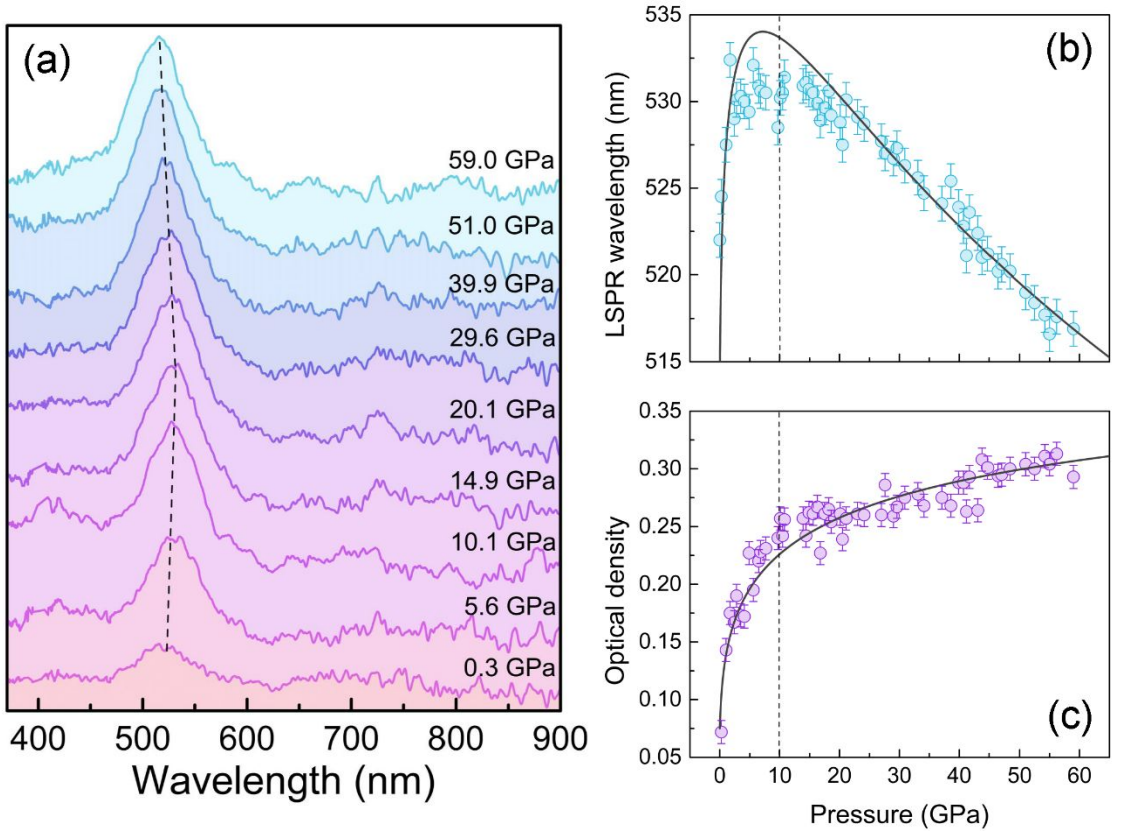

Figure 2. (a) Extinction spectra of AuNSs in MeOH-EtOH (4:1) [1×10^{13} NS/cm^3] as a function of pressure (raw data). (b) Pressure dependence of the LSPR position for AuNSs and (c) The optical density at the LSPR band maximum corrected for the sample thickness as a function of the applied pressure (t = 50 μm at ambient pressure). Plots include experimental and calculated values of $\lambda_{LSPR}(P)$ and extinction cross-section using the Gans model. Filled circles correspond to experimental data and lines represent the calculated values. Calculation details are provided in the text. The vertical dashed line shows the hydrostaticity limit of the pressure-transmitting medium (MeOH-EtOH 4:1 solution).

We interpret the results in terms of Gans' model,[15] which yields Mie's model[16] for spheres in the limit of particle size $r \ll \lambda$. Through this model we can directly correlate the pressure-induced LSPR shifts with the relative changes in AuNS volume through its equation of state (EOS), and the solvent refractive index at each pressure, through the following equation

$$\lambda_{LSPR} = \lambda_p(0)\sqrt{\frac{V}{V_0}}\sqrt{\varepsilon(0) + \frac{1-L}{L}\varepsilon_m} \qquad (1)$$

The pressure dependence of the optical density at the LSPR peak is obtained from the extinction coefficient through the equation

$$I_{LSPR} = CV\varepsilon_m^{3/2}/\lambda_{LSPR} \quad (2)$$

where $\lambda_p(0)$ and $\varepsilon(0)$ are the plasma wavelength and the dielectric constant of gold in the limit of zero wavelength, respectively. LSPR data (Figure 2) were analyzed using $\lambda_p(0) = 137$ nm and $\varepsilon(0) = 10.55$. These values are close to those reported by Johnson and Christy[17] and provide the overall best fit.L is the nanoparticle depolarization factor or shape factor, which is $1/3$ for a sphere.[18] $\varepsilon_m = n^2$ is the dielectric function of the non-absorbing medium, V and V_0 are the AuNS volume at P and ambient pressure, respectively, while C in Eq. 2 is a renormalization constant proportional to sample thickness and inversely proportional to the AuNS concentration. According to Eq. 1 the LSPR band shift with pressure is the result of two competing effects: compression of the conduction electrons, which increases the bulk plasma frequency proportionally to the square root of V/V_0 (blueshift), and the increase in solvent density, yielding an increase in ε_m(redshift). In the pressure range below ~ 10 GPa, the refractive-index-induced redshift is larger than the blueshift due to plasmon compression because the solvent has a higher compressibility than gold (AuNS) at low pressures. However, at a certain pressure, this trend can be reversed if the solvent becomes more incompressible than gold, a condition which is attained if their respective bulk modulus pressure derivatives fulfil: $K'_{0,sol} > K'_{0,Au}$.[8,12] Under such conditions, the effect of compression on the electron gas becomes more important than the solvent densification, thus leading to an LSPR blueshift. It is also important to note that the depolarization factor for AuNSs (L = 1/3) is bigger than that for AuNRs (L< 1/3), which means that spheres exhibit a weaker dependence of the LSPR to changes in solvent refractive index (see Eq. 1). From the smooth and continuous behavior of $\lambda_{LSPR}(P)$ observed over the whole pressure range (Fig. 2(b)), we infer that there is no evidence of pressure-induced solid-solid structural transitions above 10 GPa in the glass-like state of MeOH-EtOH (4:1). Moreover, we find no sign of abrupt changes in the refractive index (*i.e.* the solvent density) around the liquid-to-solid transition, as no observable jumps in $\lambda_{LSPR}(P)$ around the solidification pressureare observed. A similar conclusion was obtained from previous investigations elsewhere.[3,12] The good agreement between measured and calculated values for the LSPR shifts and the optical density at the LSPR peak as a function of pressure provides solid support for the use of the modified Gans' model.

Given the isotropy of the solvent in its liquid state, we assume that pressure does not induce reshaping of AuNSs under a hydrostatic load due to their fcc cubic lattice. In the non-hydrostatic regime this is no longer applicable, due to the appearance of anisotropic stress components. Nevertheless, according to the results shown in Fig. 2 (b and c), we conclude that such effects are negligible for AuNSs since the pressure dependence of both the measured and calculated LSPR wavelengths and the corresponding optical extinction are in fair agreement with each other, if we assume that the Au nanoparticles remain spherical and non-aggregated over the 0-60 GPa range. This result is also supported by the slight variation of the FWHM of the LSPR band with pressure (Fig. S2), which should increase considerably in aggregated or reshaped AuNS dispersions. Since the change in particle volume can be described by a first-order Murnaghan EOS

$$\frac{V}{V_0} = \left(\frac{PK'_0}{K_0} + 1\right)^{-1/K'_0} \quad (3)$$

with K_0= 190 GPa, and $K_0' = \left(\frac{\delta K}{\delta P}\right)_{P=0}$ = 6 for Au nanoparticles,[12] it is possible to infer the pressure-dependence of the solvent refractive index over the explored pressure range, by fitting the measured LSPR pressure shifts to Eq. 1 and describing the pressure dependence of the refractive index by a phenomenological Murnaghan-type equation:

$$n = n_0\left(\frac{P\alpha}{\beta} + 1\right)^{1/\alpha} \quad (4)$$

where $n_0 = 1.3274$ is the refractive index of MeOH-EtOH (4:1) at ambient pressure, and α and β are empirical fitting parameters. This method was previously used to obtain the pressure dependence of the refractive index of pure water from AuNR plasmonics.[1] The complete $\lambda_{LSPR}(P)$ data were thus fitted to Eq. 1, using Eqs. 3 and 4 to describe the pressure dependence of the gold electron density and the solvent dielectric function, respectively. For MeOH-EtOH (4:1) in the 0-60 GPa range, we obtain $\alpha = 19.3 \pm 0.6$ and $\beta = 4.3 \pm 0.5$ GPa. This procedure provides an analytical expression for $n(P)$ for the alcohol mixture over the widest pressure range ever explored. The method has the advantage that the two main contributions to the LSPR shifts are well known and can be easily decoupled since the contribution from the electronic density $N(P)$of gold is well determined from the EOS for Au nanoparticles. Figure 3 compares the $n(P)$ data obtained in this work against other experimental data reported by Eggert *et al.*,[3] Ahrens *et al.*,[4] Petersen *et al.*,[5] Vedam and Limsuwan[6] and Chen and Vedam.[7] We obtain very similar $n(P)$ values to those reported by Vedam and Limsuwan[6] in methanol in the low-pressure range ($P < 2$ GPa). At higher pressures, we observe a reasonable agreement with results from Eggert *et al.*[3] In general, we find good overall among the different data sets, with the exception of the shock data for ethanol, which shows a deviation of 5% from our data. Such a deviation with respect to $n(P)$ values derived from static pressure measurements is likely due to uncertainties in determining the instantaneous values of pressure and temperature in a shock experiment.

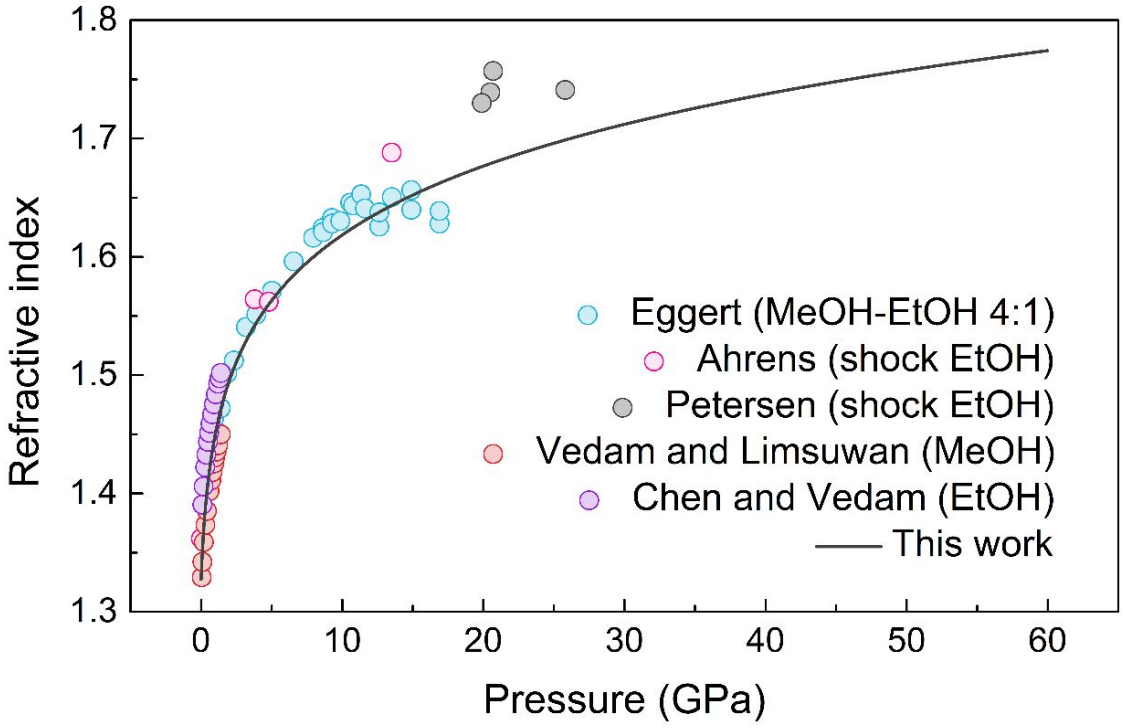

Figure 3. Pressure dependence of the refractive index of methanol-ethanol mixtures. Filled circles correspond to previously reported experimental data: (blue) Eggert *et al.*[3] in MeOH-EtOH 4:1, (pink) Ahrens *et al.*[4] and (grey) Petersen *et al.*[5] in ethanol using shock-compression methods, (red) Vedam and Limsuwan[6] in methanol and (purple) Chen and Vedam[7] in ethanol. The solid line represents the experimental refractive index values obtained in this work for MeOH-EtOH 4:1 using Eq. 4.

We can likewise use the optical data to model the changes in density in the solvent mixtures under increasing pressure, using the Lorentz-Lorentz relation:

$$\varepsilon_m(P) = n^2 = \frac{1+2u}{1-u} \tag{5}$$

where $u = \frac{4\pi N_A}{3\,V_0}\left(\frac{V_0}{V}\right)\alpha_p$. Here N_A is Avogadro's number, V_0 is the zero-pressure molar volume, and α_p is the molecular polarizability at P, which can be described phenomenologically by the equation $\alpha_p = \alpha_0\left(\frac{V_0}{V}\right)^{\varphi}$.[3] From these relationships, we calculate the pressure dependence of the MeOH-EtOH (4:1) density as:

$$\frac{\rho}{\rho_0} \propto \left(\frac{n^2-1}{n^2+2}\right)^{\frac{1}{1+\varphi}} \tag{6}$$

where $\rho_0 = 0.811$ g/cm^3 is the density at zero pressure of MeOH-EtOH (4:1).[3] We can fairly account for the pressure dependence of the optical density at the LSPR, by fitting the $I_{LSPR}(P)$ data of Fig. 2(c) with Eq. 2. We obtain a value of $\varphi = -0.08$ for MeOH-EtOH (4:1) over the whole 0-60 GPa range.

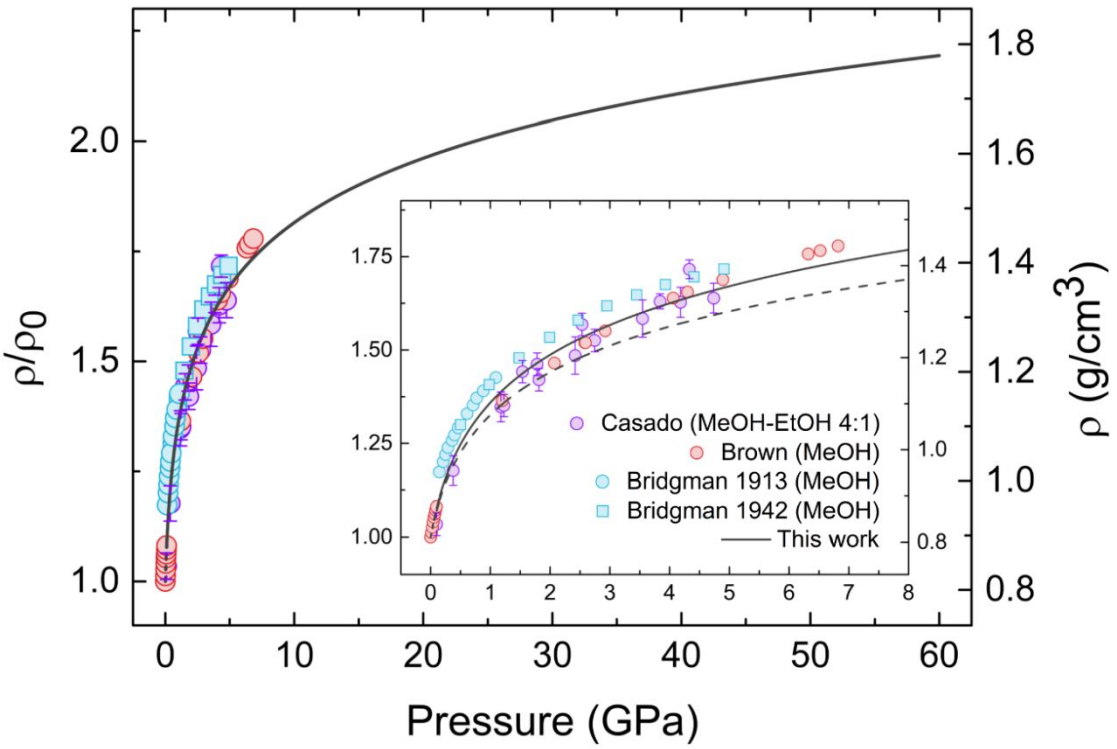

Figure 4. Pressure dependence of the density of methanol-ethanol mixtures. Filled circles correspond to experimental data: (purple) Casado *et al.*[8] in MeOH-EtOH (4:1), (red) Brown *et al.*[19] in MeOH and (blue) Bridgman[20,21] in MeOH. Solid line represents the values obtained in this work for MeOH-EtOH 4:1 using the Lorentz-Lorentz model. The dashed line represents the density values obtained from the Lorentz-Lorentz model when the geometric density dependence of the polarizability with pressure, *i.e.*$\varphi = 0$, is not taken into account.

Figure 4 compares the $\rho(P)$ values obtained using Eq. 6 with those reported by Casado *et al.*[8] in MeOH-EtOH (4:1), and by Bridgman[20,21] and Brown *et al.*[19] in MeOH. It should be noted that the fitted φ value is slightly different from the value $\varphi = -0.157$ previously found by Eggert *et al.*[3] However, this discrepancy likely arises because φ was derived from $n(P)$ values measured by interferometric methods, when working with the pure MeOH EOS obtained by Bridgman *et al.*[20] ($K_0 = 0.778$ GPa and $K'_0 = 10.18$), which slightly deviates from those reported in the literature for MeOH-EtOH (4:1) below 8 GPa (Fig. 4). This discrepancy is also reflected in the slight systematic deviation also found in the $n(P)$ values reported Eggert *et al.*[3], as shown in Fig. 3. The suitability of the Lorentz-Lorentz model to describe the pressure dependence of the MeOH-EtOH (4:1) density was checked by comparing our density values from Eq. (6) against experimental $\rho(P)$ data reported by Casado *et al.*[8] for the MeOH-EtOH (4:1) system and by Brown *et al.*[19] and Bridgman[20,21] for pure MeOH. Our model provides very similar $\rho(P)$ values as those found by Casado *et al.*[8] and by Brown *et al.*[19] although they slightly deviate from Bridgman's data[20,21], which, in view of the limited set of data, may be somewhat overestimated.

Conclusions

We have shown that the plasmonic properties of AuNSs can be used as the basis for sensing changes in the surrounding medium under very high pressure. Application of pressure to AuNSs induces LSPR shifts with two different behaviors: at low pressure (< 10 GPa) the LSPR rapidly redshifts with increasing pressure, due to the high compressibility of the solvent, and this effect is more important than the blueshift due to compression of the conduction electrons in metallic gold. Nevertheless, the LSPR behavior is reversed above 10 GPa, where pressure induces a slight blueshift. We have demonstrated that this effect is caused by the progressive hardening of the solvent with pressure, the bulk modulus of which becomes higher than that of the gold nanoparticle. At these higher pressures, the blueshift due to the increase in the gold bulk plasma frequency becomes more important than the redshift due to the increase in the solvent refractive index. We also found that pressure-induced solvent solidification has a negligible spectroscopic effect on the LSPR line shape or energy of the gold nanospheres. LSPR spectra show a smooth variation in peak wavelength over the entire 0-60 GPa range, with no evidence for solid-solid transformations in the glass-like state of MeOH-EtOH (4:1). We have shown that plasmonic sensing allows the pressure dependence of the MeOH-EtOH (4:1) refractive index to be determined, even under strongly non-hydrostatic conditions. Our $n(P)$ data were also validated against previous experimental values reported elsewhere.[3-7] We found that our model provides $n(P)$ and $\rho(P)$ over the 0-60 GPa range, which are consistent with previously reported data at much lower pressures, and therefore increase the pressure range over which high pressure experiments can be conducted quantitatively.

Supporting Information

1) Hydrostaticity of the AuNS dispersions in MeOH-EtOH (4:1) as pressure transmitting media: liquid-solid transition pressure; 2) Broadening of the localized surface plasmon resonance (LSPR) bandwidth with pressure: hydrostatic and non-hydrostatic effects.

Acknowledgements

Financial support from Projects PGC2018-101464-B-I00, MAT2017-86659-R and MDM-2017-0720 (Ministerio de Ciencia, Innovación y Universidades) and MALTA-Consolider Team (RED2018-102612-T) is acknowledged. PM acknowledges support from the ARC through grant CE170100026.

Abbreviations

AuNP, gold nanoparticle; LSPR, localized surface plasmon resonance; AuNR, gold nanorod; MeOH-EtOH, methanol-ethanol; AuNS, gold nanosphere; EOS, equation of state; DAC, diamond anvil cell.

References

[1] Martín-Sánchez, C.; González-Rubio, G.; Mulvaney, P.; Guerrero-Martínez, A.; Liz-Marzán, L. M.; Rodríguez, F. Monodisperse Gold Nanorods for High-Pressure Refractive Index Sensing. *J. Phys. Chem. Lett.***2019**, *10*, 1587-1593.

[2] Klotz, S.; Chervin, J. C.; Munsch, P.; Le Marchand, G. Hydrostatic Limits of 11 Pressure Transmitting Media. *J. Phys. D: Appl. Phys*. **2009**, *42*, 075413.

[3] Eggert, J.H.; Xu, L.; Che, R.; Chen, L.; Wang, J. High Pressure Refractive Index Measurements of 4:1 Methanol:Ethanol. *J. Appl. Phys.* **1992**, *72*, 2453.

[4] Ahrens, T. J.; Ruderman, M. H. Inmersed Foil Method for Measuring Shock Wave Profiles in Solids. *J. Appl. Phys.* **1966**, *37*, 4758.

[5] Petersen, C. F.; Rosenberg, J. T. Index of Refraction of Ethanol and Glycerol under Shock. *J. Appl. Phys.* **1969**, *40*, 3044.

[6] Vedam, K.; Limsuwan, P. Piezo and Elastooptic Properties of Liquids under High Pressure II. Refractive index vs density. *J. Chem. Phys.* **1978**, *69*, 4772.

[7] Chen, C. C.; Vedam, K. Piezo and Elastooptic Properties of Liquids under High Pressure III. Results on twelve more liquids. *J. Chem. Phys.* **1980**, *73*, 4577.

[8] Casado, S.; Lorenzana, H. E.; Cáceres, M.; Taravillo, M.: Baonza, V. G. Direct measurement of the liquid 4: 1 methanol–ethanol equation of state up to 5 GPa. *High Pressure Res*. **2008***, 28,* 637-640.

[9] Guo, L.; Jackman, J. A.; Huang-Hao, Y.; Chen, P.; Cho, N. J.; Kim, D. H. Strategies for enhancing the sensitivity of plasmonic nanosensors. *Nano Today* **2015**, *10*, 213-239.

[10] Zheng, Y.; Zhong, X.; Li, Z.; Xia, Y. Successive, Seed-Mediated Growth for the Synthesis of Single-Crystal Gold Nanospheres with Uniform Diameters Controlled in the Range of 5-150 nm. *Part. Part. Syst. Charact.* **2014**, *31*, 266–273.

[11] Syasen, K. Ruby Under Pressure. *High Pressure Res.* **2008**, *28*, 75-126.

[12] Martín-Sánchez, C.; Barreda-Argüeso, J. A.; Seibt, S.; Mulvaney, P.; Rodríguez, F. Effects of Hydrostatic Pressure on the Surface Plasmon Resonance of Gold Nanocrystals. *ACS Nano* **2019**, *13*, 498-504.

[13] Barreda-Argüeso, J. A.; Rodríguez, F. Patent No. PCT/ES2014/000049, 2013.

[14] Runowski, M.; Sobczak, S.; Marciniak, J.; Bukalska, I.; Lis, S.; Katrusiak, A. Gold Nanorods as a High-Pressure Sensor of Phase Transitions and Refractive-Index Gauge, *Nanoscale*, **2019**, *11*, 8718-8726.

[15] Gans, R. Über Die UltramikroskopischerGoldteilchen. *Ann. Phys.* **1912**, *342*, 881-900.

[16] Bohren, C. F.; Huffman, D. R. *Absorption and Scattering of Light by Small Particles*; Wiley: New York, 1983.

[17] Johnson, P. B.; Christy, R. W. Optical Constants of Noble Metals. *Phys. Rev. B,* **1972**, *6*, 4370-4379.

[18] Pérez-Juste, J.; Pastoriza-Santos, I.; Liz-Marzán, L. M.; Mulvaney, P. Gold Nanorods: Synthesis, Characterization and Applications. *Coord. Chem. Rev*. **2005**, *249*, 1870-1901.

[19] Brown, J. M.; Slutsky, L. J.; Nelson, K. A.; Cheng, L. T. Velocity of sound and equations of state for methanol and ethanol in a diamond-anvil cell. *Science*, **1988**, *241*, 65-67.

[20] Bridgman, P.W. Thermodynamic properties of twelve liquids between 20" and 80" and up to 12000 Kg/cm^2. *Proc. Am. Acad. Arts Sci.* **1913**, *49*, 3-114.

[21] Bridgman, P. W. Freezing Parameters and Compressions of Twenty-One Substances to 50000 Kg/cm^2.*Proc. Am. Acad. Arts Sci* .**1942**, *74*, 399-424.

BRIEFS. The high-pressure effects on the localized surface plasmon resonances (LSPR) of monodisperse gold nanospheres in alcohol have been measured up to 60 GPa. Pressure-induced shifts show two different regimes at low pressure (redshift) and high pressure (blueshift), the low-pressure redshift being associated with the higher compressibility of the alcohol that gold in the 0-10 GPa range. The unusual pressure-induced LSPR blueshift is provoked by the increase in electron density as metallic gold becomes softer than alcohol above 10 GPa.

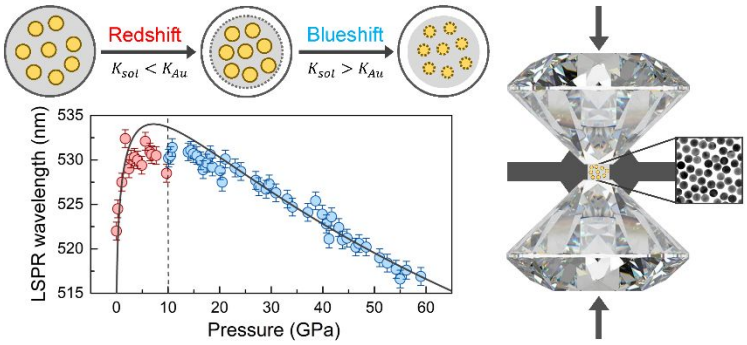
Redshift
$K_{sol} < K_{Au}$
Blueshift
$K_{sol} > K_{Au}$
LSPR wavelength (nm)
535
530
525
520
515
0
10
20
30
40
50
60
Pressure (GPa)

TOC Graphic

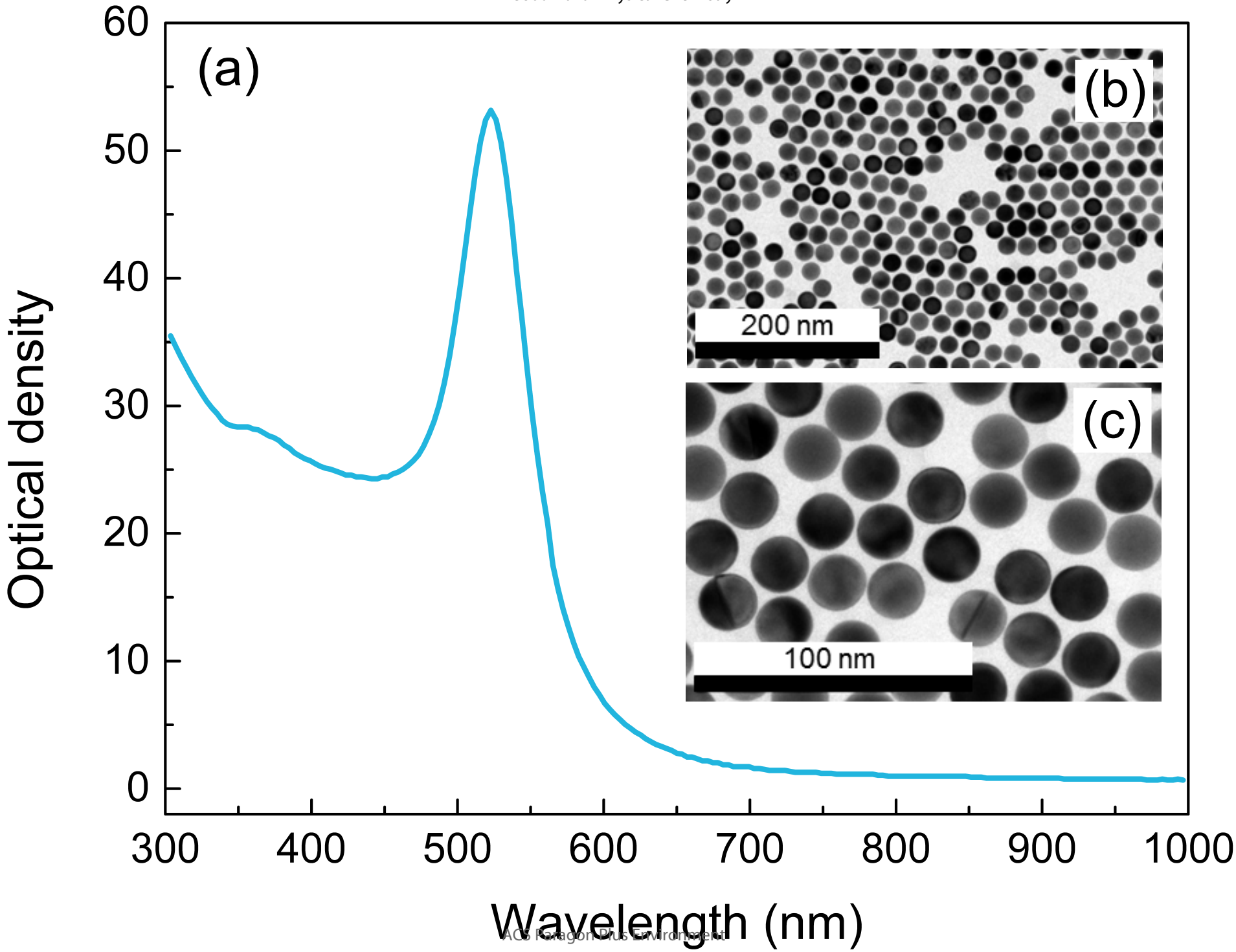

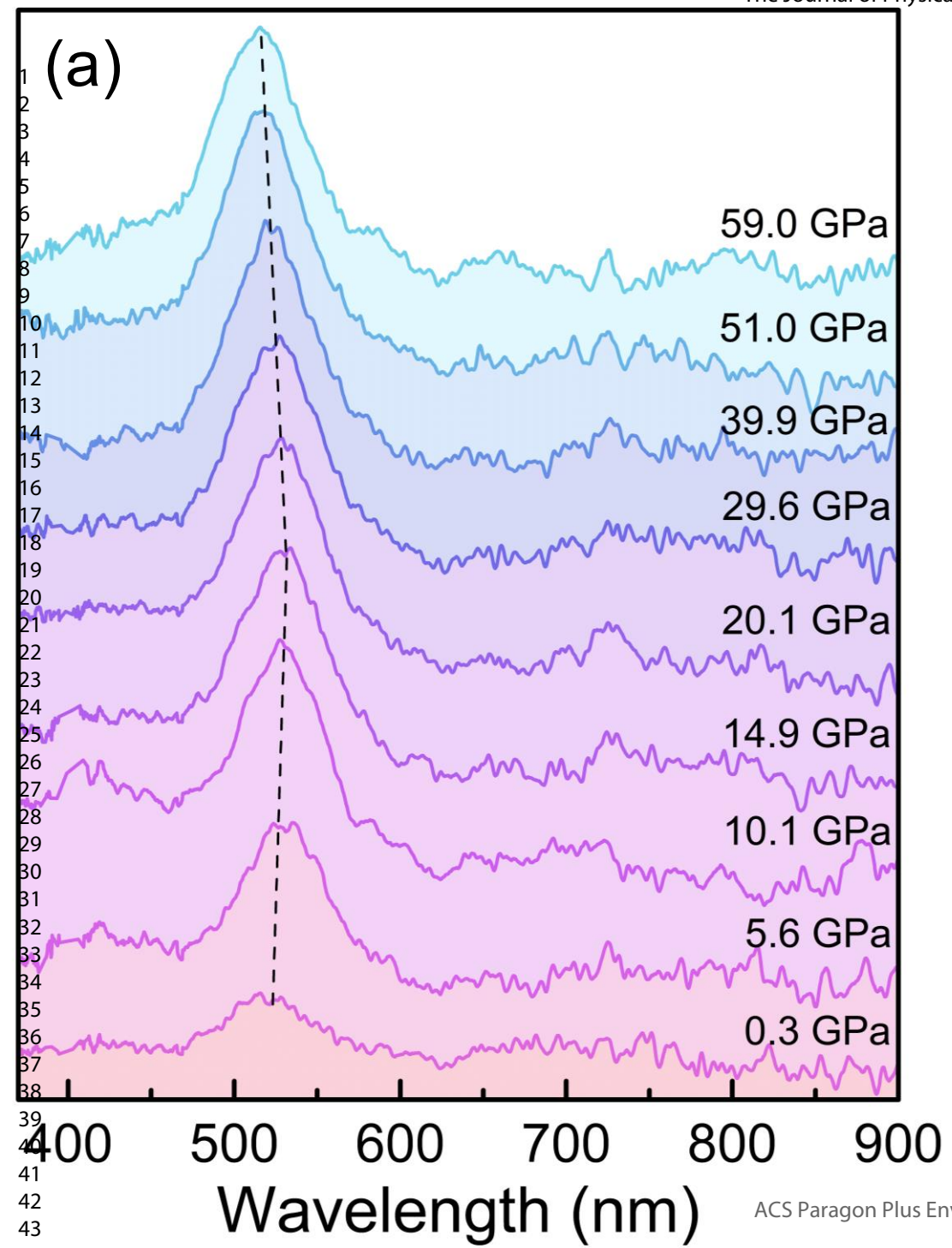
(a)
59.0 GPa
51.0 GPa
39.9 GPa
29.6 GPa
20.1 GPa
14.9 GPa
10.1 GPa
5.6 GPa
0.3 GPa
400
500
600
700
800
900
Wavelength (nm)

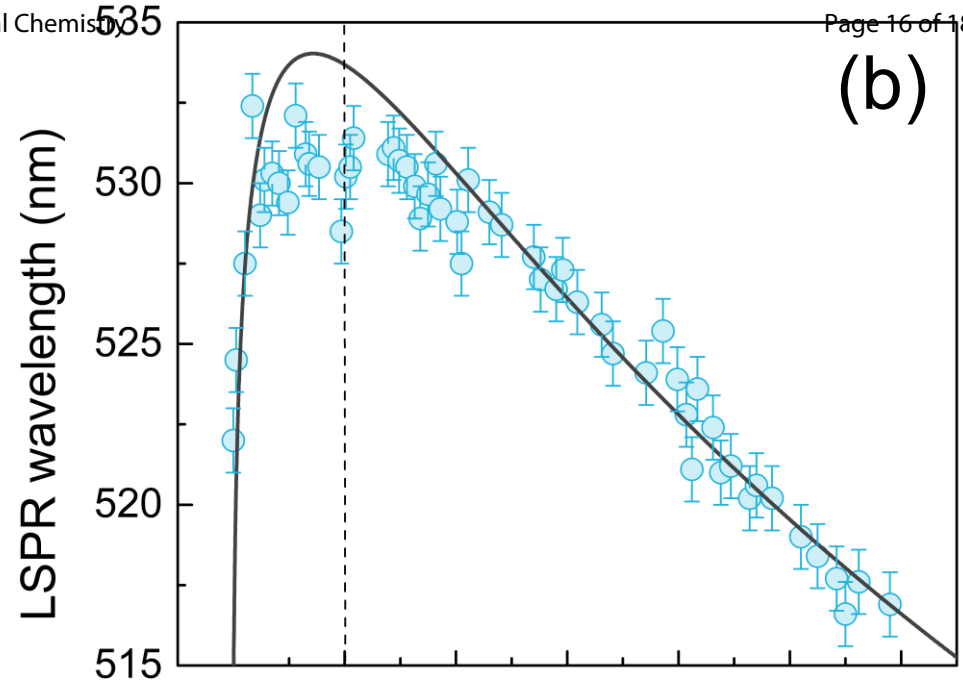
(b)
LSPR wavelength (nm)
535
530
525
520
515

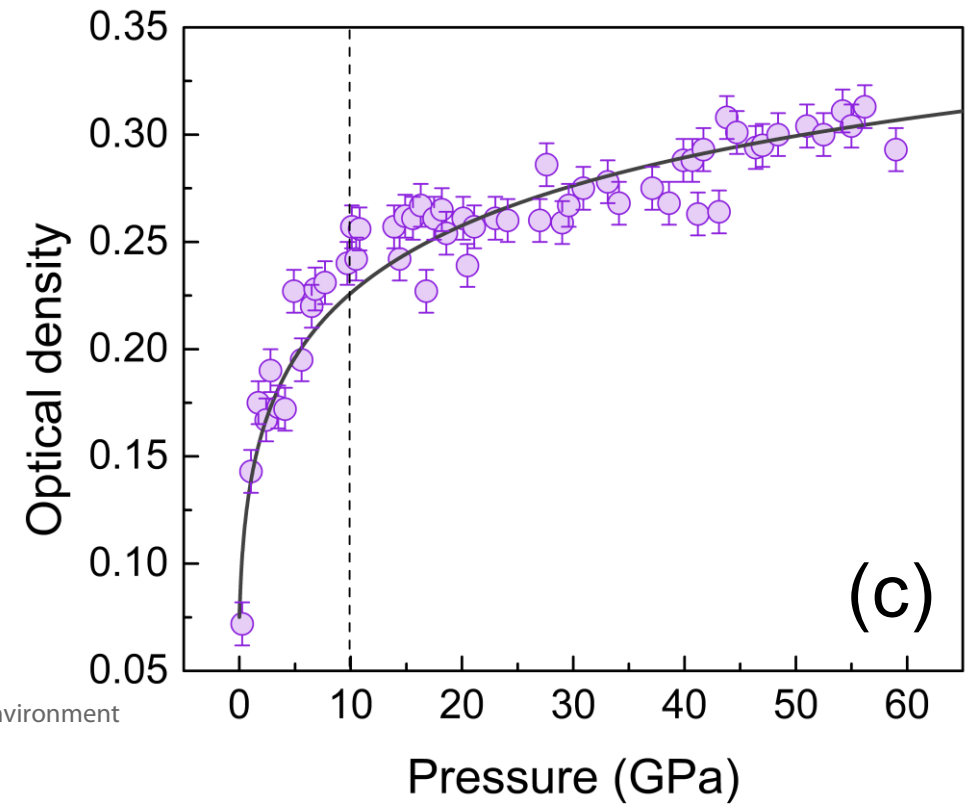
(c)
Optical density
0.35
0.30
0.25
0.20
0.15
0.10
0.05
0
10
20
30
40
50
60
Pressure (GPa)

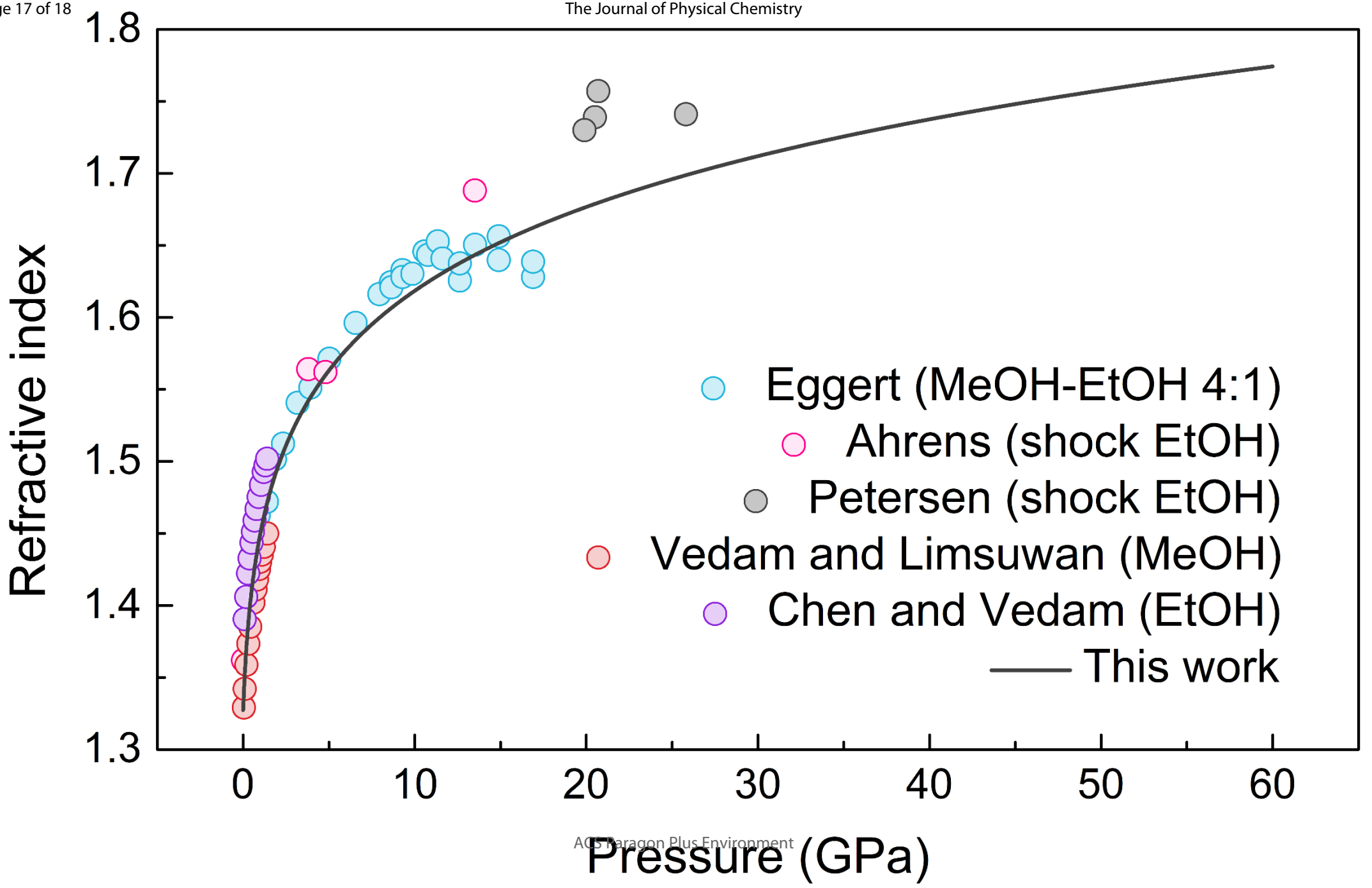

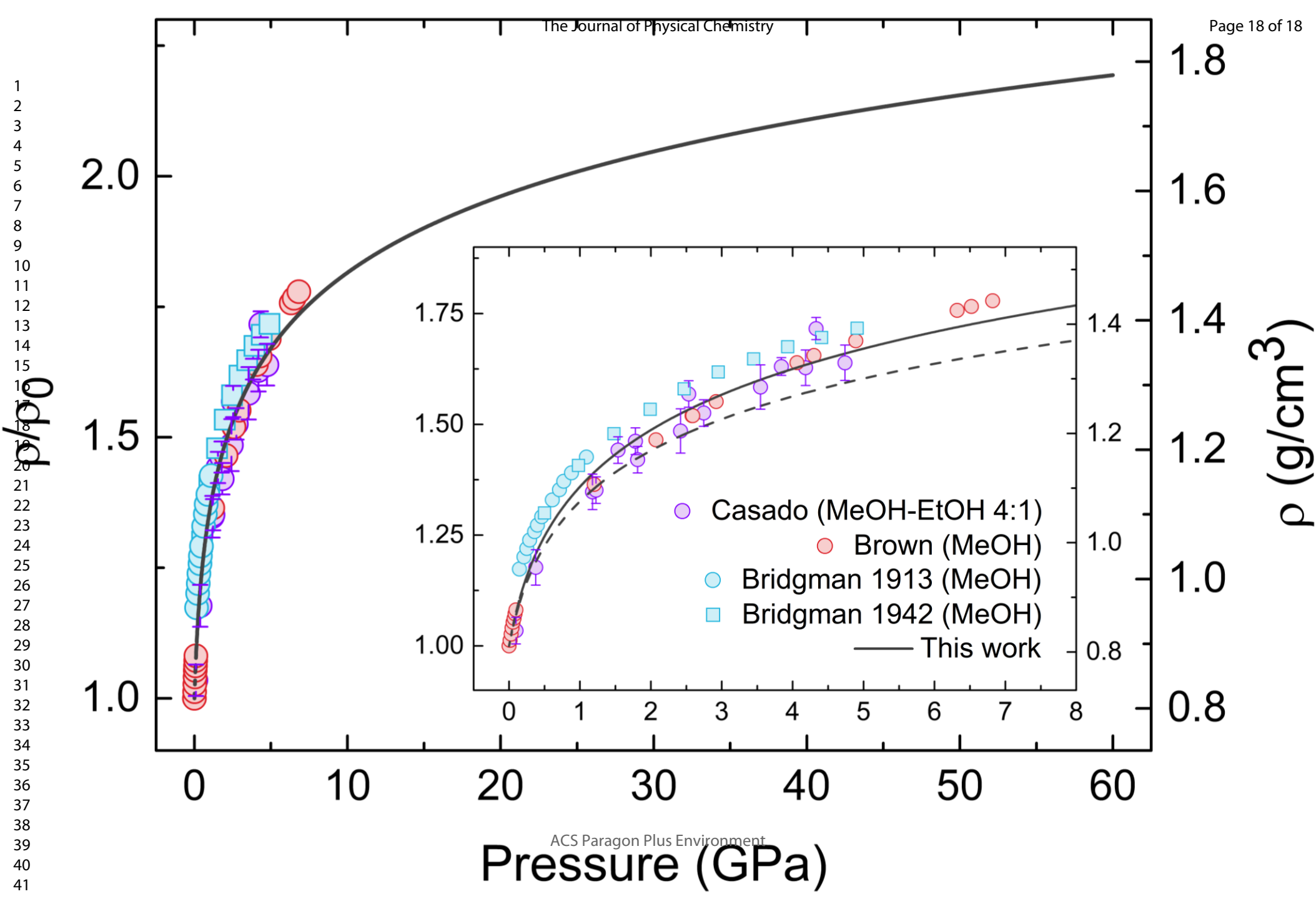
p/p0
ρ (g/cm3)
Pressure (GPa)
Casado (MeOH-EtOH 4:1)
Brown (MeOH)
Bridgman 1913 (MeOH)
Bridgman 1942 (MeOH)
This work